International Journal of Geology, Earth & Environmental Sciences ISSN: 2277-2081
An Open Access, Online International Journal Available at http://www.cibtech.org/jgee.htm
2026 Vol. 16, pp. 131-139/Thokchom et al.
Research Article

RADIOLOGICAL ASSESSMENT OF SANDSTONES IN AND AROUND GELMON, HENKOT AND TUILAPHAI OF CHURACHANDPUR DISTRICT, MANIPUR, NE-INDIA

***Thokchom Lilthoingambi Chanu[1], Khumukcham Radhapiyari Devi[2] and N. Ibotombi Singh[1]**
[1]Department of Geology, Bir Tikendrajit University (BTU), Canchipur.
[2]Department of Earth-Sciences, Manipur University, Imphal
**Author for Correspondence: lilthoingambichanu@gmail.com*

ABSTRACT
Eight sandstone samples from Gelmon, Henkot and Tuilaphai of Churachandpur District have been selected for their radiological assessment. The assessment was conducted and recorded the average value of radium equivalent (Ra_{eq}), absorbed dose (D) and Annual effective dose (D_{eff}) as 425.39±38.54 $Bqkg^{-1}$ ranging from 237.08±28.01 $Bqkg^{-1}$ - 681.55±62.94 $Bqkg^{-1}$; 201.53±18.23 $nGyh^{-1}$ ranging from 110±12.78 $nGyh^{-1}$ – 319.36±29.54 $nGyh^{-1}$; and, 1.23±0.10 $mSvy^{-1}$ ranging from 0.67±0.07 $mSvy^{-1}$ – 1.95±0.18 $mSvy^{-1}$. Some samples show maximum limit and even cross permissible limit compare to world data.

***Keyword**: Churachandpur, Sandstones, Radiological Assessment*

INTRODUCTION

It is believed that the genesis of uranium enrichment was driven by strong volcanic activity, which produced a significant amount of tuff that, when combined with air and water, was ultimately deposited alongside normal clastic sedimentary particles during the Jurassic period. Thin section analysis of these rocks reveals that well-developed tuff is present in the sandstones, with an average content of 45%. The tuff, which contains a high concentration of uranium, serves as a substantial source for uranium enrichment.

The specific levels of naturally occurring radionuclides and the associated gamma radiation depend primarily on the geographical and geological composition of each lithologically distinct separated area (Abusini M *et al.,* 2008). In other words, naturally occurring radionuclides, also known as primordial or terrestrial radionuclides, are distributed in varying amounts in the Earth's crust (Ajithra AK *et al.,* 2017) and appear at different levels of each region in the world includes the decay radionuclides in the series of Uranium (^{238}U), Thorium (^{232}Th) with their daughter progeny, and natural Potassium (^{40}K). The content of Uranium (^{238}U), Thorium (^{232}Th), and Potassium (^{40}K) of the rock is distinguished based on the types of rocks (i.e., shale, mudstone, sandstone, and clastic rocks, etc). Igneous rocks show greater radioactivity than sedimentary rocks; however, in some exceptions, shale and phosphate rocks in sedimentary rocks have relatively high radioactivity (El-Taher A & Al-Zahranj JH, 2014; Singh SN *et al.,* 2017). Among them, one of the above is considered responsible for contributing the highest amount of natural background radiation in the environment, which may be an interesting thing to know.

Natural background radiation is a major source of human exposure to ionizing radiation, which may result in an increase in health risk to humans, such as chronic diseases, when exposed above the permissible level (Alamgir Miah *et al.,* 2012). Naturally occurring radionuclides in soil contribute a significant amount of background radiation exposure to the population through inhalation and ingestion.

The natural gamma ray log measures the total spontaneous radioactivity of geological formations (Yuan R *et al.,* 2018) and radioactivity elements such as Uranium (^{238}U), Thorium (^{232}Th), and Potassium (^{40}K) with half-life which are comparable with the age of the earth (Farai IP & Vincent, UE 2006); however generally, the total spontaneous radioactivity is very significant to indicate the lithology of deep burial rocks i.e. gravelly and sandy sediments are less radioactive than silt and clay with high gamma ray (Yuan R. *et al.,* 2018).

Based on cores, open-hole conventional logs, and mineral component analysis, an abnormal natural gamma-ray log with high values in conglomerates and low values in fine-grained sediments is described and explained in the Baikouquan formation of Xiazijie Fan-delta, Mahu Depression, Junggar Basin (R. Yuan *et al.,* 2018).

A group of geologists who pioneered uranium mining brought to light many uranium occurrences in the Singhbhum Thrust Belt. The first uranium deposit discovered in 1951 in the eastern part of the country extends about 160 km, and soon it became evident that it holds the potential for commercial uranium mining operations. In the northeastern part of the country, sandstone-type uranium deposits at Domiasiat, Wahkhyn and Mawsynram in the Mahadek basin of Meghalaya (fig. 1) provide near-surface flat ore bodies amenable to commercial operations (IAEA, 2006). This deposit with large and good-grade uranium reserves is hosted in a thick pile of sandstone within a depth of about 40 m with underlying granite. The capital city, Imphal, of the state of Manipur in Northeastern India is about 300 km away from the Domiasiat (Singh SN *et al.,* 2017), which lies in the Himalayan and its tributaries region. Churachandpur district of Manipur has a geological setting of the Barail Group made up of massive to thickly bedded sandstone, alternation of sandstone and shale (Singh YR *et al.,* 2017); it also shears in a hill range extending up to Meghalaya. Therefore, it may be believed that it is necessary to estimate the amount of natural radionuclide which is containing in sandstone found in and around the Churachandpur district, Manipur, India.

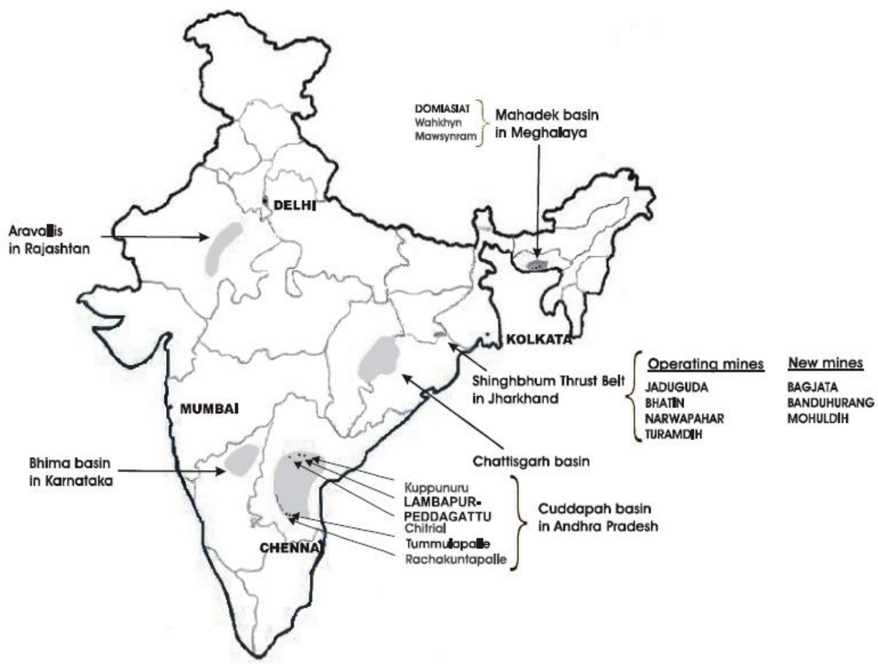

Fig. 1: Major Uranium provinces of India after R. Gupta & A.K. Sarangi, 2005 (IAEA, 2006).

GEOLOGICAL SETTING OF THE STUDY AREA

The study area covers the road section of about 30km from Churachandpur to Tuilaphai located at latitudes 24°20´- 24°25´ N and longitudes 93°35´- 93°45´ E, stretching along National Highway No. 2. The geological formations exposed in the study area include Disang Group, Barail Group and Alluvium (fig. 2). A simplified stratigraphic succession of the study area is given in table-1. The Disang Group of rocks lie unconformable just above the Basement complex. The Disangs are dominated by argillaceous rocks like shales and interbedded with flaggy sandstone. A minor amount of mudstone and siltstone is present at the lower part of the column, where bedded splintery shales and interbedded siltstone and sandstone are present at the upper part of the formation. Brachiopod fossils of Eocene age are abundantly present in the Disang shale. The Disang shales are characterised by a splintery nature due to the presence of many joints, which are the result of tectonic movements.

The Barails Group of rocks, particularly the arenaceous one, lies above the Disang Group with gradational contact. Fine to medium-grained, multi-storied bedded sandstones are well developed, interbedded with thin layers of shale Brown colour sandstones contain coal streaks/carbonaceous materials. Cross-bedding and ripple marks are the prominent structures of the rocks. Wood fossils of Oligocene age can be seen in the rocks.

The Barials rocks are unconformably overlain by a group known as alluvium. The deposits consist of dark grey to black clay, silt, and sandy deposits of fluvio-lacustrine origin.

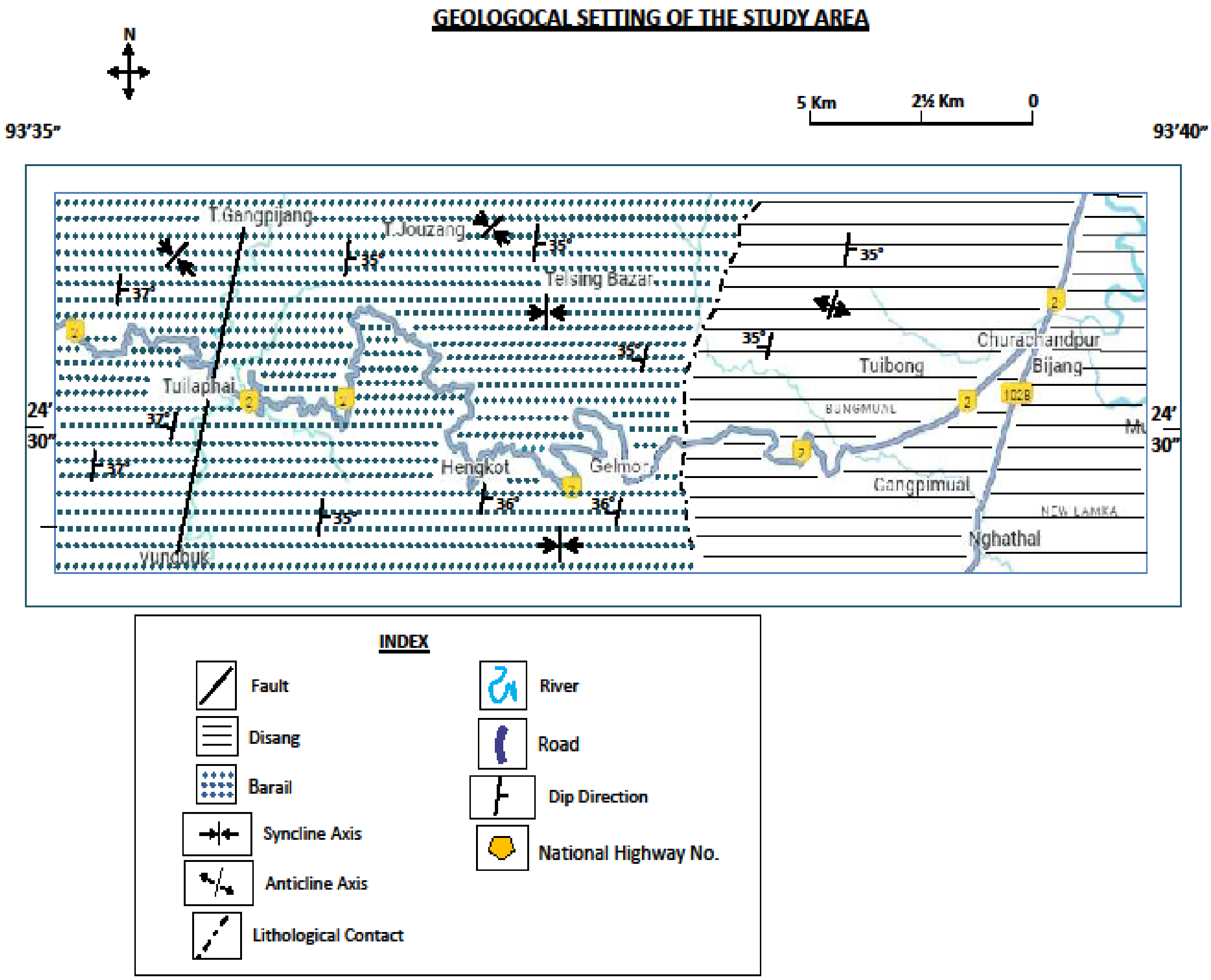

Fig. 2: Pictorial representation of geological setting of the study area

Table 1: Stratigraphic succession of the study area

	Group	Description of Rocks
Alluvium		Dark grey to black clay, silt, and sandy deposits of lacustrine origin
....Stratigraphic break...		
Oligocene	Barail Group	Fine medium grained multi-storied bedded sandstone alternated with shale. Brown colour sandstone often contained carbonaceous materials. Shale is thinly laminated.
---Gradational contact--		
Eocene	Disang Group	Dark grey splintery shale inter bedded with siltstone and fine grained sandstone. Thickness of the sandstone and siltstone are maximum at the upper part. Argillaceous dark grey shale inter-bedded with mudstone and thinly bedded the siltstone at the lower part.
--- Unconformity ---		
Basement complex		unseen

.

MATERIALS AND MATHODS

Sample Collection and Preparation

The study area was selected because of the abundance and fresh exposures of barail rocks. Approximately sandstone samples, each weighing 1 kg, were collected from 08 different sites of the study area during November, 2022 - February, 2023, to a depth of about 30 cm from the rock surface, packed inside a thick black polythene bag and brought to the laboratory for further necessary action. The samples were subjected to drying in a hot air oven at 110°C overnight (~20 h) and ground into fine powder, homogenised, and sieved through a mesh size of 0.45mm (Roth J *et al.,* 1996). 300 g of each sample were stored carefully in a non-radioactive plastic container and sealed with adhesive tape for over a period of 4 weeks at room temperature to secure equilibrium conditions of ^{226}Ra and ^{232}Th along with their respective daughter nuclides (AERB, 2003; Asaduzzaman K, 2015) by following Suranjit S *et al.*, (2020).

Radiological Assessment of Sandstones

Analysis for radionuclide concentration was performed by a 3"x 3" NaI(Tl) scintillation detector-based gamma spectrometer (Mane ST *et al.,* 2014; Ademola AK *et al.,* 2015; Rajesh S & Kerur BR, 2018) with a cylindrical lead shield of thickness about ~ 10 cm. The efficiency calibration of the gamma-ray spectrometer was made using calibrated standard source samples, which contain a known activity of gamma-ray emitters radionuclide namely ^{133}Ba (356.1 keV), ^{137}Cs (661.6 keV), ^{60}Co (1173 KeV and 1332 KeV) and ^{226}Ra (1764.5 keV) with different energy peaks covering the range up to ≈ 2000 keV by following Suranjit S *et al.,* (2020). The counting time was preset at 36,000 s (10 hrs.) to obtain the gamma spectrum with good statistics (Ademola AK *et al.,* 2015); then, background radiation was measured and subtracted from the gross count to get the net count rate for each sample (Rajesh S & Kerur BR, 2018).

Activity Concentration (A): The activity concentrations of ^{238}U, ^{232}Th series, and ^{40}K were calculated using the following equation–1;

$A\ (Bqkg^{-1}) = N/\varepsilon\beta M$ ---------------- (1)

Where, A = the activity concentration of the radionuclide in the sample given in $Bqkg^{-1}$, N = the net gamma counting rate (counts per second), ε = the detector efficiency of the specific gamma-ray, β = the absolute transition probability of gamma decay, and M = the mass of the sample in kg.

Radium Equivalent (Ra_{eq}): The relative concentration and distribution of ^{226}Ra, ^{232}Th, and ^{40}K were not uniform in the environment and were not found to be uniform in barail rocks (sandstones). Radium equivalent (Ra_{eq}) activity index is introduced to represent the specific activity of ^{226}Ra, ^{232}Th and ^{40}K by a single quantity. The index parameter Ra_{eq} is related to exposure to radiation and defined to compare the specific activity of material containing different activities of ^{226}Ra, ^{232}Th, and ^{40}K. For the uniformity in exposure estimates, the concentrations of radionuclides have been defined in terms of radium equivalent activity (Ra_{eq}) in $Bqkg^{-1}$ (NEA-OECD, 1979; Ajithra AK *et al.,* 2017) is computed by equation–2 (UNSCEAR, 1982).

$Ra_{eq} = A_{Ra} + 1.43A_{Th} + 0.077A_K$ -------------- (2)

Where, A_{Ra}, A_{Th}, and A_K are the specific activities of ^{226}Ra, ^{232}Th, and ^{40}K in $Bqkg^{-1}$, respectively.

Adsorbed Dose Rate (D): The absorbed Dose Rate due to gamma radiation in air at 1 meter above ground surface for a standard sample with naturally occurring radionuclide ^{226}Ra, ^{232}Th and ^{40}K was calculated using dose conversion factors viz 0.462 $nGyh^{-1}$ for ^{238}U series, 0.604 $nGyh^{-1}$ for ^{232}Th series and 0.042 $nGyh^{-1}$ for ^{40}K series as per the guidelines prescribed by UNSCEAR (2000) represent the equation–3.

$D\ (nGyh^{-1}) = 0.462\ A_{Ra} + 0.604\ A_{Th} + 0.042\ A_K$ -------------------- (3)

Annual Effective Dose (D_{eff}): The annual effective dose was calculated by applying the dose conversion factor of 0.7 $SvGy^{-1}$ from the absorbed dose in air received by an adult; and the value of 0.8 as an indoor occupancy factor, implying that 80% of the time in a day of an individual is spent indoors, followed by 0.2 as an outdoor occupancy (UNSCEAR, 2000).

External Hazard Index (H_{ex}): The external hazard index is an assessment of dose rate due to external hazard of the gamma radiation emitted by natural radionuclides from the sandstones, evaluated by the following equation–4 (Lu X & Xiolan Z, 2006; Alarmgir Miah *et al.,* 2012)

$H_{ex} = A_{Ra} / 370\ Bakg^{-1} + A_{Th} / 258\ Bakg^{-1} + A_K / 4810\ Bakg^{-1}$ ------------- (4)

Excess of Lifetime Cancer Risks (ELCR): Excess of lifetime cancer risks is an estimate of the probability of fatal cancer occurrence from exposure to low-level doses of radiation during a pilot's period, given by using equation–5.

$ELCR = D_{eff} \times L \times Rf$ ---------------------------- (5)

Where, L = life expectancy of Indian people is 80 years, Rf = risk factor in Sv^{-1} for public exposure is 0.05 for stochastic effect recommended by ICPR (1991); and world average value is 0.25×10^{-3} (Rashed-Nizam QM *et al.,* 2015)

RESULTS AND DISCUSSION

The activity concentration of ^{226}Ra was determined from the average activity concentration obtained from the prominent gamma lines of ^{214}Bi and ^{214}Pb, and that of ^{232}Th was obtained from the average concentration obtained from the gamma lines of ^{212}Bi, ^{228}Ac, and ^{208}Tl, respectively. However, ^{40}K was

Table 2: Shows activity concentrations (A), Radium Equivalent (Ra_{eqv}), Activity concentration index or gamma index (I) of ^{238}U, ^{232}Th and ^{40}K in the rock sample.

Sample	Activity concentration (A) ($Bqkg^{-1}$)			Ra_{eqv} ($Bqkg^{-1}$)	I
	^{226}Ra	^{232}Th	^{40}K		
GLM1-A3	36.8±1.8	044.2±1.8	2236.9±189.5	272.2	1.1
GLM1-B	41.8±3.8	129.8±10.2	2109.3±168.7	389.8	1.5
GLM2-E	61.4±2.9	214.1±17.1	2132.7±106.8	531.7	2.0
GLM2-G	46.3±4.5	092.9±12.9	0752.5±065.8	237.0	0.6
HK3-A	49.9±6.0	162.3±14.2	1773.6±192.7	418.6	1.1
HK3-B	58.4±6.4	305.1±27.1	2426.8±231.0	681.6	1.8
HK3-C	41.5±4.5	214.3±14.4	1246.0±135.3	443.9	1.2
TL4-A	78.6±7.8	168.5±23.8	1412.2±169.1	428.2	1.3

evaluated from its own gamma photopeak. All the values are given in $Bqkg^{-1}$ of dry weight of the sample. The activity concentration of ^{226}Ra were determined as the ranges from 36.8±1.8 $Bqkg^{-1}$ – 78.6±7.8 $Bqkg^{-1}$from the sample GLM1-A3and TL4-A; followed by ^{232}Th ranges from 44.2±1.8 $Bqkg^{-1}$ – 305.1±27.1 $Bqkg^{-1}$ from the sample GLM1-A3 and HK3-B; and, ^{40}K ranges from 752.5±65.8 $Bqkg^{-1}$ – 2426.8±231.0 $Bqkg^{-1}$ from the sample GLM2-G and HK3-B, respectively, shown in table 2. The activity concentration of ^{232}Th was observed to be higher than ^{238}U in all samples, which is consistent with Ajithra AK *et al.,* (2017), who revealed that due to the presence of black sands, which are enriched in the mineral monazite containing a significant amount of ^{232}Th.

The radium equivalent (Ra_{eqv}) of ^{226}Ra, ^{232}Th, and ^{40}K from all samples were varied from 237.08±28.01 $Bqkg^{-1}$ - 681.55±62.94 $Bqkg^{-1}$ with an average value of 425.39±38.54 $Bqkg^{-1}$ is slightly higher than the threshold value of 370 $Bqkg^{-1}$ (NEA-OECD, 1979; UNSCEAR 1982) which gives an annual dose rate of 1 $mSvy^{-1}$ (Singh SN *et al.,* 2017). Ra_{eqv} is the most widely used radiation hazard index parameter for materials containing ^{226}Ra, ^{232}Th and ^{40}K (table 3).

The absorbed dose (D) rate were recorded in a ranged from 110±12.78 $nGyh^{-1}$ to 319.36±29.54 $nGyh^{-1}$ with an average value of 201.53±18.23 $nGyh^{-1}$ seems to be higher than the world average dose rate of 59 $nGyh^{-1}$ recommended by UNSCEAR (2000); permissible limits of 84 $nGyh^{-1}$ and 90 $nGyh^{-1}$ for Global and Indian dose rates, respectively (table 3).

The average annual effective dose was recorded as 1.23±0.10 $mSvy^{-1}$ (table 3), which is slightly higher than the worldwide permissible limit of 1.1 $mSvy^{-1}$ prescribed by UNSCEAR (2000); and the maximum permissible dose limit for non-radionuclide industrial workers and public as 1 $mSvy^{-1}$ recommended by ICPR (1991 & 2007). The minimum and maximum annual effective doses were estimated in a range from 0.67±0.07 $mSvy^{-1}$ to 1.95±0.18 $mSvy^{-1}$ (chart 1).

The average value of external Hazard Index (H_{ex}) was recorded as 1.14±0.09, which is slightly greater than 1. This index value must be less than unity for the radiation hazard to be neglected or insignificant (Ajithra AK *et al.,* 2017); that means the area is safe for humans to live (Alarmgir Miah *et al.,* 2012). The maximum value of H_{ex} must be less than unity for the radiation hazard, which corresponds to the upper limit of Ra_{eqv} of 370 $Bakg^{-1}$ (table 3).

The Excess Lifetime Cancer Risk (ELCR) is the probability of a fetal cancer occurrences as a result of exposure to the low level natural background radiation of general public or individual during their lifetime (more than over 20 years) (Paschal I. Enyinna, 2016) was estimated in a range from 2.69 x 10^{-3} – 7.8 x 10^{-3} with an average value of 4.93 x 10^{-3} which is much higher than the world average value is 0.25 x 10^{-3} (UNSCEAR, 2000) (table 3).

Table 3: Shows Average values of Absorbed Dose (Abs. Dose), Effective Dose (Eff. Dose), Hazard Index (H_{ex}) and Excess Lifetime Cancer Risk (ELCR) and Permissible limits to general public prescribed by UNSCEAR (2000) and ICRP (2007).

Sl. No.	**Sample**	**Ra_{eqv} ($Bqkg^{-1}$)**	**Gamma Index (I) ($Bqkg^{-1}$)**	**Abs. Dose ($nGyh^{-1}$)**	**Eff. Dose ($mSvy^{-1}$)**	**Hazard Index** (H_{ex})	**ELCR (x 10^{-3})**
1	GLM1-A3	272.24	1.1	139.43	0.85	0.73	3.42
2	GLM1-B	389.83	1.5	189.41	1.16	1.05	4.64
3	GLM2-E	531.78	2.0	251.31	1.54	1.43	6.16
4	GLM2-G	**237.00**	**0.6**	**110**	**0.67**	**0.64**	**2.69**
5	HK3-A	418.60	1.1	198.68	1.21	1.13	4.87
6	HK3-B	**681.55**	**1.8**	**319.36**	**1.95**	**1.84**	**7.8**
7	HK3-C	443.89	1.2	204.8	1.25	1.19	5.02
8	TL4-A	428.29	1.3	199.26	1.22	1.15	4.88
Average Value		**425.39**	**1.3**	**201.53**	**1.23**	**1.14**	**4.93**
International Permissible Limit		**370**	**--**	**60**	**1**	**≤ 1**	**0.29 x 10^{-3}**

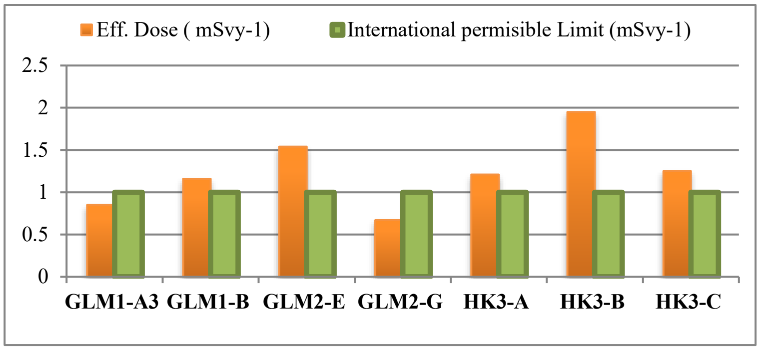

Chart 1: Graphical representation between Eff. Dose and International Permissible Limit.

CONCLUSION

Background radiation contributed by naturally occurring radionuclides such as ^{238}U, ^{232}Th, and ^{40}K was estimated by a NaI(Tl) based gamma spectrometer. Moreover, this study showed a wide distribution of radionuclide activity concentration among the samples. The sedimentary rocks, i.e., sandstone samples collected from Gelmon, Tuilaphai, and Henkot of Churachandpur district, Manipur, showed higher thorium (Th) activity than radium (Ra) activity, which is leached out with water but remains in soil. Most of the samples showed high potassium (K) activity concentration. The present study revealed that absorbed and effective doses are slightly higher than the international or worldwide permissible limit. This study is aimed at academic research purposes.

ACKNOWLEDGMENTS

The present study is the outcome of the investigations carried out by the authors. The authors express gratitude to the Dept. of Geology, Bir Tikendrajit University (BTU), Imphal; the Dept. of Geology, D. M. College of Science, Dhanamanjuri University (DMU); and the Dept. of Physics, National Institute of Technology, Imphal, for providing laboratory support necessary for this study.

FINANCIAL SUPPORT AND SPONSORSHIP

Nil

CONFLICTS OF INTEREST

There are no conflicts of interest.

REFERENCES

Abusini M, Al-Ayasreh K, Al-Jundi J (2008). Determination of Uranium, Thorium and Potassium activity concentrations in soil cores in Araba valley, Jordan. *Radiation Protection Dosimetry*. **128**(2) 213-216. https://doi.org/10.1093/rpd/ncn276

Ademola, Augustine & Olaoye, Morounfolu & Abodunrin, Oluwasayo (2015). Radiological safety assessment and determination of heavy metals in soil samples from some waste dumpsites in Lagos and Ogun state, South-western, Nigeria. *Journal of Radiation Research and Applied Sciences*. **11**(1) 148-153. 10.1016/j.jrras.2014.12.010.

Ajithra AK, Venkatraman B, Jose MT, Chandrasekar S, Shanthi G (2017). Assessment of natural radioactivity and associated radiation indices in soil samples from the high background radiation area, Kanyakumari district, Tamil Nadu, India. *Radiation Protection and Environment*. **40**(1) 27-33. DOI: 10.4103/rpe.RPE_31_16

Alamgir Miah, Miah MMH, Masud Kamal, Chowdhury MI & Rahmatullah M (2012). Natural radioactivity and associated dose rates in soil samples of Malnichera Tea Garden in Sylhet District of Bangladesh. *Journal of Nuclear and Particle Physics*. **2**(6) 147-152. 10.5923/j.jnpp.20120206.03.

Alarmgir Miah, Miah MMH, Masud Kamal, Chaowdhury MI, Rahmatullah M (2012). Natural radioactivity and associated dose rates in soil samples of Malnichera tea garden in Sylhet district of Bangladesh. *Journal of Nuclear and Particle Physics*. **2**(6) 147-152. 10.5923/j.jnpp.20120206.03

Asaduzzaman K, Mannan F, Khandaker MU, Farook MS, Elkezza A, Amin YB, Sharma S, & Abu Kassim HB (2015). Assessment of natural radioactivity levels and potential radiological risks of common building materials used in Bangladeshi dwellings. *PloS one*. **10**(10), e0140667. https://doi.org/10.1371/journal.pone.0140667

Atomic Energy Regulatory Board (AERB) (2003). Accreditation of laboratories for measurement of radionuclide content in commodities. Atomic Energy Regulatory Board, Mumbai, India.

El-Taher A & Al-Zahrani JH (2014). Radioactivity measurements and radiation dose assessments in soil of Al-Qassim region, Saudi Arabia. *Indian Journal of Pure and Applied Physics*. **52**(3) 147-152.

Farai IP and Vincent UE (2006). Outdoor radiation level measurement in Abeokuta, Nigeria by thermoluminiscent dosimetry. *Nigerian Journal of Physics*. **18**(1) 121-126.

IAEA (2006). Uranium production and raw materials for the nuclear fuel cycle- supply and demand, economics, the environmental and energy security. Emerging trend of uranium mining: the Indian scenario. *Proceedings of An International Symposium, Vienna, 20–24 June 2005*. Nuclear Fuel Cycle and Materials Section, International Atomic Energy Agency (IAEA), Wagramer Strasse 5, P.O. Box 100, A-1400 Vienna, Austria.

ICPR (1991). 1990 Recommendations of the International Commission on Radiological Protection. ICPR Publication 60. *Annals of the ICRP*. **21**(1-3), 1–201.

ICPR (2007). The 2007 Recommendation of the International Commission on Radiological Protection. ICPR Publication 103. *Annals of the ICPR*. **37**(2-7), 1-328

Lu X, & Zhang X (2006). Measurement of natural radioactivity in sand samples collected from the Baoji Weihe Sands Park, China. *Environmental Geology*. **50**(1) 977-982.

Mane ST, Mane TB, & Sharma A (2014). Environmental natural gamma radiation level and activity of Uranium-238, Thorium-232 at different places measured using NaI(Tl) Scintillation Detector. *International Journal of Science and Research*. **3**(12) 297-302.

Mao ZQ, Shen B, Kuang LC, Sun ZC, Luo XP (2013). The special lithologic sections of Permian Xiazijie formation in Junggar Basin: geophysical characteristics and origin. *Xinjiang Petroleum Geology*. **34**(1) 98-100.

NEA-OECD (1979). Exposure to radiation from natural radioactivity in building materials. Nuclear Energy Agency (NEA). *Report by NEA Group of experts*. Organization for economic Co-operation and Development (OECD), Paris, France.

Paschal Ikenna Enyinna (2016). Radiological risk assessment of cosmic radiation at aviation altitudes (a trip from Houston Intercontinental Airport to Lagos International Airport). *Journal of Medical physics*. **41**(3) 205-209. https://doi.org/10.4103/0971-6203.189491

Rajesh S & Kerur BR (2018). Assessment of natural radioactivity levels due to ^{238}U, ^{232}Th and ^{40}K in the soil samples of Raichur district, Karnataka, India. *Radiation Protection and Environment.* **41**(1) 51-54. 10.4103/rpe.RPE_16_18

Rashed-Nizam QM, Rahman MM, Kamal M, & Chowdhury MI (2015). Assessment of radionuclides in the soil of residential areas of Chittagong metropolitan city, Bangladesh and evaluation of associated radiological risk. *Journal of Radiation Research*. **56**(1) 22-29. https://doi.org/10.1093/jrr/rru073.

Roth J, Schweizer P, Gückel C (1996). Basis of radiation protection. *Schweizerische Medizinische Wochenschrift*. **126**(26) 1157-1171.

Singh SN, Sharma BA, Devi TP (2017). Study of natural radioactivity (^{226}Ra, ^{232}Th and ^{40}K) in soil sample for the assessment of average effective dose and radiation hazard parameter. *Radiation Protection Environment*. **40**(1) 154-158.

Singh YR, Singh BP, and Ranjeeta DS (2017). Source rock characterization, digenesis and depositional environment of the upper disang formation from Gelmoul area of Manipur, NE India. *Journal of Indian Association of Sedimentologists*. **34**(1&2) 1-7.

Sun P, Zhang XL, Guo L, Shen YB (2010). Genesis of the sandstone with higher radioactivity and the qualitative evaluation of its reservoir property: taking Chang 6 oil-bearing strata in Zhidan Oilfield, Ordos Basin as an example. *Journal of Xi'an Shiyou University (Natural Science Edition)*. **25**(2) 18-21.

Suranjit S, Singh OS, Singh SN, Sharma BA (2020). Assessment of radioactivity of different types of houses in Imphal city, Manipur, India. *Radiation Protection Environment.* **43**(1) 26-30.

UNSCEAR (1982). Ionizing radiation: Sources and Biological Effects. *1982 Report to General Assembly (A/37/45) and Twelve Scientific Annexes*. United Nations Scientific Committee of the Effect of Atomic Radiation. United Nations Publication, New York, United States of America.

UNSCEAR (2000). Source and Effects of Ionizing Radiations. *2000 Report to General Assembly (A/55/46) and Five Scientific Annexes*.. United Nations Scientific Committee of the Effect of Atomic Radiation. United Nations Publication. New York, United States of America. **Volume-1 Sources.**

Yuan R, Zhu R, Qu J, You X, Wu J, Huang Y (2018). Abnormal open-hole natural gamma ray (GR) log in Baikouquan formation of Xiazijie Fan-delta, Mahu Depression, Junggar Basin, China. *Open Geosciences*. **10**(1) 844-854. https://doi.org/10.1515/geo-2018-0066